TECHNISCHE UNIVERSITÄT DRESDEN

Form factor models and branching fractions of B meson decays in the SHERPA simulation

Bachelor-Arbeit
zur Erlangung des Hochschulgrades
Bachelor of Science
im Bachelor-Studiengang Physik

vorgelegt von

Kien Dang Tran
geboren am 16.05.1995 in Dresden

Institut für Kern- und Teilchenphysik
Fachrichtung Physik
Fakultät Mathematik und Naturwissenschaften
Technische Universität Dresden

Eingereicht am 30. Mai 2016

1. Gutachter: Dr. Frank Siegert
2. Gutachter: Prof. Dr. Kai Zuber

Kurzfassung

Deutsch:
Das Ziel dieser Bachelorarbeit ist es, eine verbesserte Simulation des B Mesonenzerfalls in der SHERPA Software zur Verfügung zu stellen. Das HADRONS++ Modul, das für die Modellierung von Hadronenzerfällen verantwortlich ist, erhält aktualisierte Verzweigungsverhältnisse und ein neues Formfaktormodell für den Zerfall von B Mesonen. Die veränderte Version wird mit der unveränderten Version in verschiedenen Zerfallssimulationen verglichen, um zu zeigen, dass die Änderungen eine Verbesserung darstellen.

Abstract

English:

The aim of this bachelor thesis is to provide an enhanced simulation of the B meson decay in the SHERPA software. The HADRONS++ module, which is responsible for modeling hadron decays, is getting updated branching fractions and a new form factor parametrization for decays of B mesons. The changed version is compared to the unchanged version in various decay simulations to show that the adjustments are an improvement.

Contents

1 Introduction

In the past two decades, particle accelerators such as the LHC (Large Hadron Collider), located in CERN, Switzerland, have become of primary interest in searching for elementary particles and understanding their nature. By accelerating charged particles and colliding them near the speed of light, a wide spectrum of particles can be created. To identify the spectrum, the detectors are made of many layers which ensure that the particles cause a signal in the detector. Particles which interact with the detector material create traces, e.g. through electromagnetic or hadronic showers, making it possible to gain information about their momenta and energies. An event in the ATLAS detector, which is one of the four main detectors of the LHC, is pictured in Fig. 1.1 where the four muons resulting from the collision are highlighted as blue lines.

The discovery of the Higgs boson, made at the LHC in 2012, is one of the biggest achievements in particle physics. The Higgs mechanism explains how fermions gain their mass and how gauge bosons can have a mass greater zero within the Standard Model. The Standard Model describes the electromagnetic, weak and strong interaction in a consistent theory, but leaves out gravitation, indicating that it is not yet complete. Quarks, which belong to the group of elementary particles, are known to interact with all four forces. So far, only bound states of quarks, called hadrons, have been observed. The B meson, which consists of a (anti)bottom quark and a lighter quark, bonded via the strong interaction, is one of the many particles created in collision events and usually decays before it reaches the detector. To simulate hard collisions, many Monte Carlo event generators have been developed over time. The very first multi-purpose event generators were originally written in the programming language Fortran like the popular program PYTHIA[1] (formerly known as Pythia/Jetset). In recent years, new ones appeared, like for example SHERPA[2] (**S**imulation of **H**igh-**E**nergy **R**eactions of **PA**rticles) which has been written in C++ from scratch. In addition to collision events, the SHERPA software can separately simulate decays of unstable hadrons, including B mesons.

The aim of this bachelor thesis is to provide an enhanced simulation of B meson decays in the SHERPA software by updating the stored branching fractions and by implementing a new form factor model. The outline of the thesis is as follows: The upcoming chapter 2 discusses the theoretical principles on which this work is based. The implementation of new form factor models and other improvements can be found in chapter 3. Afterwards, the results of the changes that were made are discussed in chapter 4. And finally, the last chapter summarizes the main findings and gives a brief outlook on the potential for further improvements.

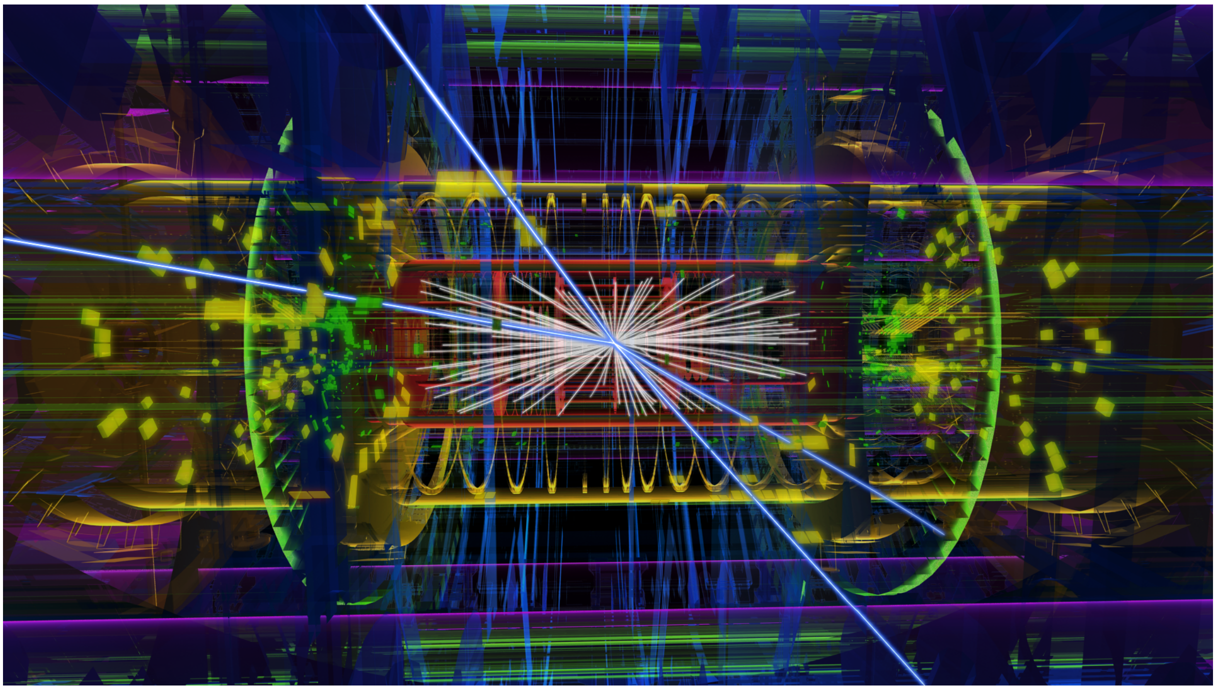

Figure 1.1: An event in the ATLAS detector is illustrated graphically where the tracks of four muons are emphasized as blue beams[3]

2 Theoretical background

2.1 The B meson

Because of the color confinement, it is not possible to observe freely propagating quarks or gluons, thus only color neutral bound states, named hadrons, can be observed. Those which consist of one quark and one antiquark, bound by the strong interaction, are called mesons. The B mesons contain one anti-bottom quark $\bar{b}$ and either an up, down, strange or charm quark. They are shown in Tab. 2.1 with their respective masses and mean lives. All of them have Spin $S = 0$, negative parity ($J^P = 0^-$) and thus belong to the group of pseudoscalar mesons. A bound state between a top and a bottom quark is not considered possible since the enormous mass of the top results in a very short life span. The lifetime of the B_c^+ is significantly shorter than the others because it contains two heavy quarks ($\bar{b}c$) which are very likely to decay by the weak interaction, whereas the others have a lightweight quark in addition to the $\bar{b}$ quark. Moreover, all of the B mesons listed in Tab. 2.1 possess a corresponding antiparticle partner named B^-, $\bar{B}^0$, $\bar{B}_s^0$ and B_c^- with adjoint quark content.

Table 2.1: List of various B mesons[4]

Symbol	**Constituents**	**Mass in MeV**	**Mean life in ps**
B^+	$\bar{b}u$	5279.29 ± 0.15	1.638 ± 0.004
B^0	$\bar{b}d$	5279.61 ± 0.16	1.520 ± 0.004
B_s^0	$\bar{b}s$	5366.79 ± 0.23	1.510 ± 0.005
B_c^+	$\bar{b}c$	6275.1 ± 1.0	0.507 ± 0.009

2.2 The decay process

The decays of N particles can be described by the decay law which is given by the following differential equation:

$$\dot{N}(t) = -\frac{\Gamma}{\hbar} \cdot N(t) = -\Gamma \cdot N(t) \qquad \text{(in natural units)} \tag{2.1}$$

with Γ being called the decay width. The solution of this equation reads:

$$N(t) = N_0 e^{-\Gamma t} \equiv N_0 e^{-t/\tau} \tag{2.2}$$

where τ is called the mean life. Most particles have more than one final state which they can decay into (decay channel), thus each channel can be identified by a partial decay width Γ_j so that the total decay width is the sum of them:

$$\Gamma \equiv \Gamma_{\text{total}} = \sum_{i=1}^{n} \Gamma_i \tag{2.3}$$

The calculation of the decay width in the non-relativistic limit can be expressed by Fermi's golden rule in the perturbation theory, but for decays of heavy particles, special relativity has to be taken into account. With that in mind, the differential decay width for a $1 \to n$ decay reads:

$$\mathrm{d}\Gamma = \frac{|\mathcal{M}|^2}{2 \cdot m_0}\, \mathrm{d}\Phi(p_1, ..., p_n) \tag{2.4}$$

so that the decay width is the integral of $\mathrm{d}\Gamma$ over the phase spaces of all the final state particles:

$$\Gamma = \int \frac{|\mathcal{M}|^2}{2 \cdot m_0}\, \mathrm{d}\Phi(p_1, ..., p_n) \tag{2.5}$$

with p_0 referring to the decaying particle, $p_1, ..., p_n$ belonging to the final state ones, and $\mathrm{d}\Phi$ being the Lorentz invariant phase space element[5]:

$$\mathrm{d}\Phi(p_1, ..., p_n) = \delta^4 \left(p_0 - \sum_{i=1}^{n} p_i \right) \prod_{i=1}^{n} \frac{\mathrm{d}^4 p_i}{(2\pi)^4} \delta(p_i^2 - m_i^2) \Theta(E_i) \tag{2.6}$$

$\mathcal{M}$ is the matrix element which can be derived from the Feynman rules. The integral for a $1 \to 2$ process is effectively two dimensional because of the four-momentum conservation and the mass shell of each particle. But for three end products, the degrees of freedom increase to five and therefore the momenta of the outgoing particles are less restricted. In this case, it is important to repeat the decay simulation of the parent particle several times to obtain proper distributions.

In weak decays of quarks, the flavour is generally not conserved. For example, the strangeness is not conserved in the $K^- \to \pi^0 e^- \bar{\nu_e}$ decay where the strange quark s couples to an up quark u through the W^- boson. Cabibbo suggested that quarks which participate in the weak interactions are a superposition of quarks involved in the strong interactions. The original idea was for two quark generations, but this was later extended to three generations in the CKM (Cabibbo, Kobayashi and Maskawa) model[6]. The weak and mass eigenstates of three generations can be expressed via the unitary matrix V_{CKM}:

$$\underbrace{\begin{pmatrix} d' \\ s' \\ b' \end{pmatrix}}_{\text{weak eigenstates}} = \underbrace{\begin{pmatrix} V_{ud} & V_{us} & V_{ub} \\ V_{cd} & V_{cs} & V_{cb} \\ V_{td} & V_{ts} & V_{tb} \end{pmatrix}}_{=:V_{\mathrm{CKM}}} \underbrace{\begin{pmatrix} d \\ s \\ b \end{pmatrix}}_{\text{mass eigenstates}} \tag{2.7}$$

with d', s', b' denoting the weak eigenstates and d, s, b labeling the mass eigenstates. The coefficients of the matrix can be complex, but relevant for the decay widths are the absolute values which are listed below[7]:

$$|V_{\mathrm{CKM}}| = \begin{pmatrix} 0.97427 \pm 0.00014 & 0.22536 \pm 0.00061 & 0.00355 \pm 0.00015 \\ 0.22522 \pm 0.00061 & 0.97343 \pm 0.00015 & 0.0414 \pm 0.0012 \\ 0.00886 \pm 0.00033 & 0.0405 \pm 0.0012 & 0.99914 \pm 0.00005 \end{pmatrix} \tag{2.8}$$

2.3 Main types of B meson decays

In this section, the semileptonic, leptonic and hadronic decays are discussed briefly because they represent the main decay types of the B meson.

2.3.1 Semileptonic decays

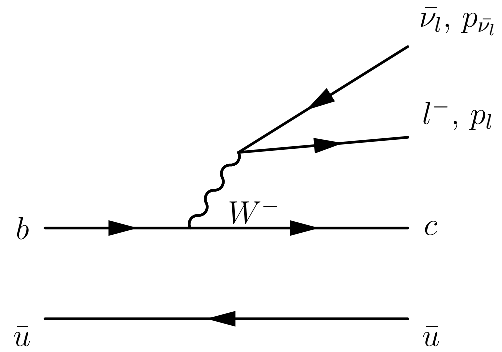

Figure 2.1: $B^- \to D^{(*)} l^- \bar{\nu}_l$ semileptonic decay

In Fig. 2.1 the semileptonic $B^- \to D^{(*)} l^- \bar{\nu}_l$ decay channel, using the $\bar{u}$ as a spectator, is illustrated as a primary example of a flavour changing weak interaction. Either the four-momenta p_l, $p_{\bar{\nu}_l}$ of the outgoing leptons or the four-momenta of the two mesons p_{B^-}, $p_{D^{(*)}}$ can be used to construct the so called momentum transfer q:

$$q = p_l + p_{\bar{\nu}_l} = p_{B^-} - p_{D^{(*)}} \tag{2.9}$$

Another variable commonly used in the literature is w, which uses the four-velocities

v_{B^-}, $v_{D^{(*)}}$ and is related to q^2 as follows:

$$w := v_{B^-} \cdot v_{D^{(*)}} = \frac{m_{B^-}^2 + m_{D^{(*)}}^2 - q^2}{2m_{B^-}m_{D^{(*)}}} \tag{2.10}$$

The matrix element for such a process is [8, Chapter 2.1]:

$$\mathcal{M}(B^- \to D^{(*)}l^-\bar{\nu}_l) = V_{cb} \cdot \left(\frac{-ig}{2\sqrt{2}}\ J_1^\mu\ \frac{g_{\mu\nu} - \frac{q_\mu q_\nu}{m_W^2}}{q^2 - m_W^2}\ \frac{-ig}{2\sqrt{2}}\ J_2^\nu \right) \tag{2.11}$$

with J_1^μ, J_2^ν denoting the electroweak hadronic and leptonic currents, V_{cb} referring to the matrix element of the CKM matrix and g being the weak coupling constant. In most cases, the squared momentum transfer q^2 will be much smaller than the squared mass m_W^2 of the W-boson, since $m_W \approx 80.4$ GeV. Hence, the W boson propagator can be approximated, resulting in the Fermi point-like interaction:

$$\mathcal{M} \approx V_{cb} \cdot \frac{G_F}{\sqrt{2}} J_1^\mu J_{2,\mu} \tag{2.12}$$

where $G_F := \frac{\sqrt{2}}{8}\frac{g^2}{m_W^2}$ is the Fermi coupling constant. Since both currents appear factorized in the matrix element, the two can be worked out independently. For this instance, the leptonic current $J_{2,\mu}$, according to the Feynman rules, reads as follows:

$$J_{2,\mu} = \langle l|\, \gamma_\mu(1-\gamma_5)\, |\bar{\nu}_l\rangle = \bar{u}(p_l)\gamma_\mu(1-\gamma_5)v(p_{\bar{\nu}_l}) \tag{2.13}$$

with u, v representing the Dirac spinors. For a $b \to c$ transition, the hadronic current can be written as:

$$J_1^\mu = \left\langle D^{(*)}(p_{D^{(*)}}) \middle| \underbrace{\bar{c}(\gamma^\mu - \gamma^\mu\gamma^5)b}_{=(V-A)^\mu} \middle| B^-(p_{B^-}) \right\rangle \tag{2.14}$$

In the literature, the term in between the bra and ket is often referred to as V - A current. In addition, the bottom quark b can also undergo a $b \to u$ transformation, only this is less likely because of the significantly smaller $|V_{ub}|$ matrix element. The problem occurring in the hadronic current J_1^μ is that the strong interaction between the quarks has to be taken into account which makes the calculation noticeably more difficult. The strong coupling constant $\alpha_s(q^2)$ becomes large for low momentum transfers q which means that the decay kinematics (Feynman diagrams) of higher orders would have to be considered as well. As a consequence, analytical solutions can not be found. The approach for this problem is to form Lorentz invariant structures based on the four-momenta p_{B^-}, $p_{D^{(*)}}$ of the mesons plus coefficient functions which depend solely on q^2. Those functions are called form factors and are similar to those required to describe atomic scattering in nuclear physics. If the outgoing meson has Spin $S > 0$, then its polarization has to be taken into account as well.

2.3.2 Leptonic decays

The leptonic decay modes of the $B^{\pm}$ mesons are suppressed, or rather they have small branching fractions $\mathcal{B}_{B\to l\nu_l}$. The branching ratio (BR) is defined as:

$$\mathcal{B}_i = \frac{\Gamma_i}{\Gamma_{\text{total}}} \tag{2.15}$$

where i denotes the decay channel. One reason for the suppression is the small $|V_{ub}|$ matrix element, visible on the left vertex in Fig. 2.2 for the $B^- \to l^-\bar{\nu}_l$ decay, which reduces the probability of such decays noticeably. Another reason is apparent in the massless limit which is relevant for e^- or μ^-. In the Standard Model, the W boson couples to left-handed fermions and right-handed antifermions. If $m \to 0$, then the eigenstates of the helicity

$$\hat{h} := \frac{\hat{\vec{S}} \cdot \vec{p}}{|\vec{p}|} \tag{2.16}$$

becomes equivalent to the eigenstates of the chirality operator γ^5. In the center of mass frame of the B^- meson, l^- and $\bar{\nu}_l$ would have momenta pointing in opposite directions and parallel spin directions because of the positive helicity of $\bar{\nu}_l$ and the negative helicity of l^-. This contradicts the fact that B^- has $S = 0$. Because e^-, μ^- and τ^- are not massless, it is possible for them to flip their helicity, allowing the decay, but with a very low probability especially for electrons.

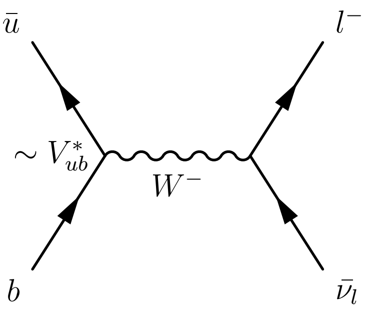

Figure 2.2: $B^- \to l^-\bar{\nu}_l$ leptonic decay

2.3.3 Hadronic decays

Purely hadronic decays, e.g. the $B^+ \to \bar{D}^0\pi^+\pi^0$ decay pictured in Fig. 2.3 (a), are very complicated to model because there are at least two currents with quarks involved. This leads to strong interactions between them, thus factorizing the currents is generally not possible. However, to simulate the hadronic decays in first approximation, the strong interaction among the currents can be ignored. Going even further, the intermediate interactions in the creation process of the pions are disregarded as well. As a result, the factorization effect in the matrix element can be regained. Then, the event can be split into $B \to D$ and $0 \to \pi\pi$. In case of the former, the form factor parameterizations as introduced in 2.3.1 can be used again for calculating the current. As for the latter, the hadronic current from the $\tau \to \nu\pi\pi$ decay, demonstrated in Fig. 2.3 (b), is being inserted to model the outgoing pions. More information about the implementation of hadronic currents resulting from tau-decays in SHERPA can be read in [9].

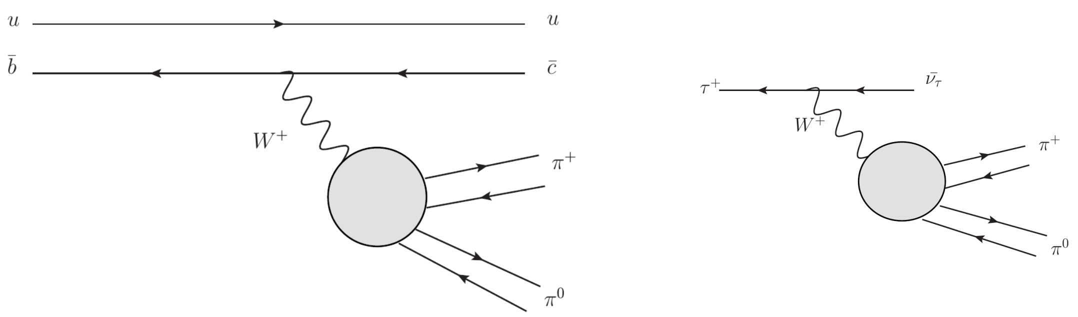

(a) $B^+ \to \bar{D^0}\pi^+\pi^0$ **(b)** $\tau^+ \to \bar{\nu_\tau}\pi^+\pi^0$

Figure 2.3: For the $B^+ \to \bar{D^0}\pi^+\pi^0$ decay (a), the hadronic currents involving pions can be extracted from the $\tau^+ \to \bar{\nu_\tau}\pi^+\pi^0$ decay (b) because the creation process of the pions can be neglected in first approximation (grey bubble).

2.4 Hadronic currents and introduction to form factor models

The hadronic current can be divided into three types depending on the spin of the outgoing meson:

- pseudoscalar $\to$ pseudoscalar ($S = 0$)
- pseudoscalar $\to$ vector ($S = 1$)
- pseudoscalar $\to$ tensor ($S = 2$)

For the pseudoscalar $P \to$ pseudoscalar P' case, the two common parametrizations are[10],[11]:

$$
\begin{aligned}
J_\mu(p_0, p_1) &= \langle P'(p_1)| (V - A)_\mu |P(p_0)\rangle \\
&= f_+(q^2)\left[(p_0 + p_1)_\mu - \frac{m_0^2 - m_1^2}{q^2} q_\mu\right] + f_0(q^2)\left[\frac{m_0^2 - m_1^2}{q^2} q_\mu\right] \qquad (2.17) \\
&= F_+(q^2)(p_0 + p_1)_\mu + F_-(q^2) q_\mu \qquad (2.18)
\end{aligned}
$$

where f_0, f_+, F_+ and F_- are the form factors and can be transformed into each other in the following way:

$$f_+ = F_+ \; ; \; f_0 = \frac{q^2}{m_0^2 - m_1^2} F_- + F_+ \tag{2.19}$$

If the decay is of the type $P \to P' l \nu_l$ (excluding the tau-leptons), the second term in the equation (2.18) can be dropped because of the small momentum transfer q_μ which means that the current becomes:

$$J_\mu(p_0, p_1) \approx F_+(q^2)(p_0 + p_1)_\mu = f_+(q^2)(p_0 + p_1)_\mu \tag{2.20}$$

As a result of the approximation, there is only one form factor f_+ left to calculate.
In the case of pseudoscalar $P \to$ vector V, the complex conjugated polarisation vector ϵ^* is needed because the resulting particle is a vector meson. With that in mind, the conventional parametrization reads[10]:

$$\begin{aligned} J_\mu(p_0, p_1) = &\langle V(p_1, \epsilon)| \, (V - A)_\mu \, |P(p_0)\rangle \\ = &\frac{2}{m_0 + m_1} \epsilon_{\mu\nu\rho\sigma} \epsilon^{*\nu} p_0^\rho p_1^\sigma V(q^2) - i \epsilon_\mu^* (m_0 + m_1) A_1(q^2) \\ &+ i \frac{\epsilon^* \cdot q}{m_0 + m_1} (p_0 + p_1)_\mu A_2(q^2) - i \frac{2 m_1 \epsilon^* \cdot q}{q^2} q_\mu (A_0(q^2) - A_3(q^2)) \end{aligned} \tag{2.21}$$

with V, A_0, A_1, A_2 and A_3 representing the form factors. The pseudoscalar $\to$ tensor transition will not be further discussed here, though more information can be found in [11].

2.4.1 The CLN model

For $B \to D^{(*)}$ currents, Caprini, Lellouh, and Neubert (CLN) introduced a form factor parametrization[12] based on the heavy quark effective theory (HQET) in 1998. The idea is to make a Taylor series expansion in $z := \frac{\sqrt{w+1} - \sqrt{2}}{\sqrt{w+1} + \sqrt{2}}$ at near zero recoil ($z \to 0$), with the result that the form factor f_+ becomes:

$$f_+(z) = V_1(1)(1 - \rho^2 z + (51\rho^2 - 10)z^2 - (252\rho^2 - 84)z^3) \tag{2.22}$$

Both ρ^2 and $V_1(1)$ are free parameters which have to be extracted from experiments. Similar derivations can be done for the pseudoscalar $\to$ vector transition. Then, the parametrizations of the obtained form factors read:

$$V(q^2) = \frac{R_1}{R^*} h_{A1} \tag{2.23}$$

$$A_0(q^2) = 0 \tag{2.24}$$

$$A_1(q^2) = \frac{1 - \frac{q^2}{(m_0+m_1)}}{R^*}\ h_{A1} \tag{2.25}$$

$$A_2(q^2) = \frac{R_2}{R^*}\ h_{A1} \tag{2.26}$$

with h_{A1}, R_1, R_2 and R^* being defined as:

$$h_{A1}(w) = h_{A1}(1)\left[1 - 8\rho^2 z(w) + (53\rho^2 - 15)z^2(w) - (231\rho^2 - 91)z^3(w)\right] \tag{2.27}$$

$$R_1(w) = R_1(1) - 0.12(w-1) + 0.05(w-1)^2 \tag{2.28}$$

$$R_2(w) = R_2(1) + 0.11(w-1) - 0.06(w-1)^2 \tag{2.29}$$

$$R^* = \frac{2\sqrt{m_0 m_1}}{m_0 + m_1} \tag{2.30}$$

In this instance, ρ, $R_1(1)$ and $R_2(1)$ are free parameters and the remaining parameter $h_{A1}(1)$ normalizes the form factors. Note that the ρ here is not the same as in equation (2.22).

2.4.2 The BGL parametrization

The BGL (Boyd, Grinstein and Lebed) ansatz[13], which is further refined by Becher and Hill[14], is another way to parametrize the form factors via a series expansion for $B \to D^{(*)} l\nu_l$ and $B \to \pi l\nu_l$ decays. The expansion is made around $q^2 = t_0$ in the semileptonic region so that the coefficients of the series become fit parameters. Because of singularities resulting from intermediate particles in the decay process, such as B^*, the convergence of the series is not yet sufficient. Therefore, the approach is a transformation of $q^2 \to z$ which is defined as

$$z(q^2, t_0) := \frac{\sqrt{t_+ - q^2} - \sqrt{t_+ - t_0}}{\sqrt{t_+ - q^2} + \sqrt{t_+ - t_0}} \tag{2.31}$$

where $t_\pm := (m_B \pm m_X)^2$ and m_X refers to the mass of the outgoing meson. The mapping shifts the whole q^2 plane from $-\infty < q^2 < t_+$ to $-1 < z < 1$. This means that the singularities are transferred to the unit disc $|z| < 1$. The constraints gathered from dispersion relations lead to the inequality:

$$\frac{1}{2\pi i}\int_C \frac{1}{z}|\phi(z, t_0)F(z, t_0)|^2 \,\mathrm{d}z \leq 1 \tag{2.32}$$

where C is the contour of the unit circle and ϕ is a weighting function which has to be analytic on the unit disk. For pions, the ϕ_+ is commonly expressed as[15]:

$$\begin{aligned}\phi_+(q^2, t_0) =& \sqrt{\frac{1}{32\pi\chi_J^{(0)}}} \left(\sqrt{t_+ - q^2} + \sqrt{t_+ - t_0}\right) \left(\sqrt{t_+ - q^2} + \sqrt{t_+ - m_-}\right)^{3/2} \\ &\times \left(\sqrt{t_+ - q^2} + \sqrt{t_+}\right)^{-5} \frac{(t_+ - q^2)}{(t_+ - t_0)^{1/4}}\end{aligned} \tag{2.33}$$

$\chi_J^{(0)}$ portrays the dispersion relation and has to be calculated numerically. In this case, $\chi_J^{(0)} = 6.889 \times 10^{-4}$[15]. Now expanding the product $P\phi F$ around t_0 yields:

$$P(q^2)\phi(q^2, t_0)F(q^2) = \sum_{k=0}^{\infty} a_k(t_0)[z(q^2, t_0)]^k \tag{2.34}$$

$$\Rightarrow F(q^2) = \frac{1}{P(q^2)\phi(q^2, t_0)} \sum_{k=0}^{\infty} a_k(t_0)[z(q^2, t_0)]^k \tag{2.35}$$

where $P(q^2) = \prod_j z(q^2, q_j^2)$ is the Blaschke factor and each q_j^2 represents a resonance. P has to be analytic on the disk $|z| < 1$ as well and its function is to regard the poles for $q^2 < t_+$. Inserting equation (2.34) into (2.32), the result is that the coefficients a_k have to satisfy

$$\sum_{k=0}^{\infty} |a_k|^2 \leq 1. \tag{2.36}$$

With this constrain the convergence of the series is sufficient, therefore taking only the first two or three orders of the series will be enough.
The parametrization is not yet available in SHERPA, though there are values available for the fit parameters. Hence, the implementation of this model is of particular interest.

2.5 The event generator SHERPA

SHERPA[2] is a multi-purpose Monte Carlo event generator which can simulate several particle collisions, e.g. hadron-hadron, lepton-lepton or hadron-lepton. As such, it consists of many modules which handle different tasks, but they are also able to interact with each other. For example, matrix elements for scattering processes can be generated via the AMEGIC++[16] module. Moreover, the tools function is to create parton level events in the SHERPA simulation which then have to be hadronised through the AHADIC++[17] component. Decays of unstable hadrons are handled by the HADRONS++[2] module and thus it will be the main focus of the upcoming chapters. The module is able to simulate the decays in respect of the given branching fractions and chosen form factor models. With the help of the form factors, it calculates the matrix element which is needed for the calculation of the differential decay width $d\Gamma$. The computation of the decay kinematics follows a simple scheme[5]. First, the phase space points $(p_1, ..., p_n) \in \Phi$ will be chosen based on the algorithm called Rambo[18]. Then the ratio

$$R := \frac{d\Gamma(p_1, ..., p_n)}{\max\limits_{x\in\Phi} d\Gamma(x)} \tag{2.37}$$

will be calculated and compared to a random value $r \in [0, 1)$. If $R > r$, the event will be accepted, otherwise the process will be repeated.

A hadron-hadron collision simulation is shown in Fig. 2.4. The big dark green arrows on the left and right side of the picture indicate the incoming partons. At parton level, the red process in the center shows the associated production of a top quark pair with a Higgs boson, which then proceed to decay because of their short lifetime, creating quarks and leptons. Furthermore, the whole event involves multiple QCD bremsstrahlung which afterwards generate additional parton showers in the event, as well as QED bremsstrahlung. As a consequence of the color confinement, the outgoing quarks will eventually hadronise (indicated by the light green ellipses) to stable or unstable hadrons, since free quark states and gluons have not been observed yet. This is illustrated as outer phase, also referred to as hadron level, where the decaying hadrons are portrayed by the dark green circles.

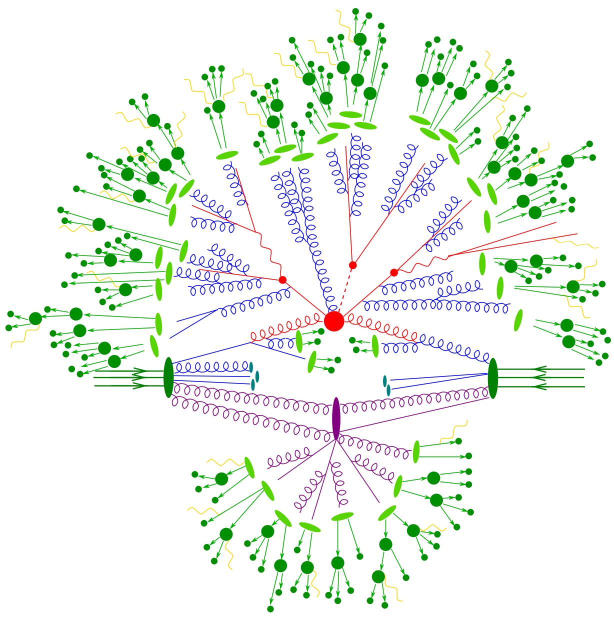

Figure 2.4: An illustration of the production of a top quark pair with a Higgs boson (red) as an inner product of a hadron-hadron scattering (big dark green arrows). Shortly, the top pair and Higgs boson decay which leads to parton showers and afterwards to hadronisation processes (light green ellipses). Some of the resulting hadrons decay further (dark green circles) and do not reach the detector. The purple colored process is a secondary hard interaction which happens simultaneously, but is not of particular interest.[2]

3 Implementation and phenomenological studies

3.1 Updating the branching fractions

In the HADRONS++ module, the decay information of known unstable hadrons are stored as a database file (`Decaydata.db`). The data file was extracted by the `Db2Dir` script for easy editing. For each hadron listed in the `Decaydata` folder there exists a `Decays.dat` file which covers most of the available branching ratios (BR) listed on the Particle Data Group website[4] (PDG). PDG is an international organisation of physicists who evaluate and reanalyze various publications with respect to particle physics. In SHERPA, the latest updates of the branching fractions of the $B^{\pm}$ and B^0 are from the PDG table of 2006, but for the B_s^0 meson, the numbers are picked from 2012. Hence, it is necessary to update the BR's of the most frequent or easily measured decay channels to obtain accurate calculations of the decay kinematics. With that said, PDG's live updated site from March 2016 is used to refresh the data. For this 3 month period, it should be noted that it takes too much work to match all the numerated branching ratios of the decay channels listed in PDG with SHERPA, since they handle included decays in different ways. Unwanted double weighting of the same decay channel could potentially happen. Because of the strong similarities between the $B^{\pm}$ and B^0 in respect of their decay products and partial decay widths, the following conclusions and adjustments for $B^{\pm}$ are also applicable to B^0. In most cases this is reasonable because both contain a first generation quark which are interchangeable if the decay is viewed at tree level.

On that account, the first part that has to be updated for $B^{\pm}$ are the semileptonic decays because a lot of them contribute a big part to the full width Γ. For example, the $B^+ \to D^* l^+ \nu_l$ decay has a BR of 5.69%. Here, l denotes only electrons and muons, but not tau-leptons because they are much heavier than the former two and as a consequence, they have to be viewed separately. Furthermore, charged leptons are well measurable in detectors which is why the uncertainties for most of those channels are very low and thus justifying the adjustments.

The modifications which were made to the semileptonic/leptonic decay modes for B^+

Table 3.1: Changes in the semileptonic/leptonic branching fractions

BR before	BR after	Change in %	Decay channel
0.065 ± 0.005	0.0569 ± 0.0019	-12.5	$B^+ \to \bar{D}^*(2007)l^+\nu_l$
0.016 (EvtGen)	0.0188 ± 0.002	+17.5	$B^+ \to \bar{D}^*(2007)\tau^+\nu_\tau$
0.0215 ± 0.0022	0.0227 ± 0.0011	+5.6	$B^+ \to \bar{D}^* l^+\nu_l$
0.007 (EvtGen)	0.0077 ± 0.0025	+10	$B^+ \to \bar{D}^*\tau^+\nu_\tau$
0.0053 ± 0.0010	0.0042 ± 0.0010	-20.8	$B^+ \to D^-\pi^+l^+\nu_l$
0.0064 ± 0.0015	0.0061 ± 0.0006	-4.7	$B^+ \to D^-(2010)\pi^+l^+\nu_l$
7.40e-05 ± 1.10e-05	7.80e-05 ± 0.27e-05	+5.4	$B^+ \to \pi^0 l^+\nu_l$
8.00e-05 ± 4.00e-05	3.80e-05 ± 0.60e-05	-52.5	$B^+ \to \eta l^+\nu_l$
8.40e-05 (EvtGen)	2.30e-05 ± 8.00e-06	-72.6	$B^+ \to \eta' l^+\nu_l$
1.24e-04 ± 0.23e-4	1.58e-04 ± 0.11e-04	+27.4	$B^+ \to \rho(770)l^+\nu_l$
3.80e-07 ± 0.90e-07	5.50e-07 ± 0.70e-07	+44.7	$B^+ \to K^+e^+e^-$
3.80e-07 ± 0.90e-07	4.43e-07 ± 0.24e-07	+16.6	$B^+ \to K^+\mu^+\mu^-$
7.30e-07 ± 5.40e-07	1.55e-06 ± 0.40e-06	+112.3	$B^+ \to K^{*+}(892)e^+e^-$
8.64e-05	1.14e-04 ± 0.27e-04	+31.9	$B^+ \to \tau^+\nu_\tau$

are shown in Tab. 3.1 with their respective BR's before and now and also their relative change in percentage. Some values prior to this were gathered from EvtGen[19], which is a B meson Monte Carlo event generator, instead of PDG because at that time there weren't any decent measurements yet for those specific decays. Even though the uncertainties are not used in the calculations of SHERPA, it is remarkable that they have been reduced significantly in almost all decays in the past ten years. In other words, the newer values should be better suited for computations.

Regarding the hadronic ones, all the $B^+ \to \bar{D}^{(*)}X$ decays, where X represents either D mesons or pions, are updated, since they have fairly big branching ratios. Moreover, those with up to three pions in addition to the $\bar{D}^{(*)}$ meson should be calculable as discussed in chapter 2.3.2 and thus are also considered in the BR update. Tab. 3.2 displays the adjustments that are made for $B^+ \to \bar{D}^{(*)}X$ modes, but also demonstrates a new decay channel $B^+ \to \bar{D}^*(2007)\pi^+\pi^+\pi^-\pi^0$ which is implemented for the B^+ meson because its branching ratio is relatively high with $(1.8 \pm 0.4)\%$. For now, this decay is handled by the generic matrix element until a suitable parametrization is found. In the case of the B^0 meson, the corresponding channel $B^0 \to D^{*-}(2010)\pi^+\pi^+\pi^-\pi^0$ is already implemented. Apparently, some of the BR's predicted by EvtGen almost match the current results from experiments, therefore showing how accurate simulations can be.

By looking at the data of the B_s^0 meson, it is noticeable that there have not been many evaluations yet for its partial decay widths because they are not as easy to produce as the $B^\pm$ or B^0 mesons. As it stands, some of the decay channels are adjusted to match the PDG table. The changes are listed in Tab. 3.3.

Table 3.2: Changes in the hadronic branching fractions

BR before	**BR after**	**Change in %**	**Decay channel**
1.09e-02 ± 0.27e-02	9.00e-03 ± 0.90e-03	-17.4	$B^+ \to D_s^+ \bar{D}^0$
1.00e-02 ± 0.40e-02	8.20e-03 ± 1.70e-03	-18.0	$B^+ \to D_s^+ \bar{D}^*(2007)$
7.20e-03 ± 0.26e-02	7.60e-03 ± 1.60e-03	+5.6	$B^+ \to D_s^{*+} \bar{D}^0$
2.20e-02 ± 0.70e-02	1.71e-02 ± 0.24e-02	-22.3	$B^+ \to D_s^{*+} \bar{D}^*(2007)$
4.80e-04 ± 1.00e-04	3.80e-04 ± 0.40e-04	-20.8	$B^+ \to \bar{D}^0 D^+$
4.92e-03 ± 0.20e-03	4.81e-03 ± 0.15e-03	-2.2	$B^+ \to \bar{D}^0 \pi^+$
4.60e-03 ± 0.04e-03	5.18e-03 ± 0.26e-03	+12.6	$B^+ \to \bar{D}^*(2007)\pi^+$
11.535e-02 (EvtGen)	5.7e-03 ± 2.2e-03	-50.6	$B^+ \to \bar{D}^0 \pi^+\pi^+\pi^-$
8.985e-03 (EvtGen)	1.03e-02 ± 0.12e-02	+14.6	$B^+ \to \bar{D}^*(2007)\pi^+\pi^+\pi^-$
1.5e-02 (EvtGen)	1.5e-02 ± 0.7e-02	±0	$B^+ \to \bar{D}^{*-}(2010)\pi^+\pi^+\pi^0$
1.7e-03 (EvtGen)	1.55e-03 ± 0.21e-03	-8.8	$B^+ \to \bar{D}^0 D^+ K^0$
1e-02 (EvtGen)	9.2e-03 ± 1.2e-03	-8.0	$B^+ \to \bar{D}^*(2007) D^{*+}(2010) K^0$
1.5e-03 (EvtGen)	1.45e-03 ± 0.33e-03	-3.3	$B^+ \to D^0 \bar{D}^0 K^+$
0.7e-02 (EvtGen)	1.12e-02 ± 0.13e-02	+60.0	$B^+ \to D^*(2007) \bar{D}^*(2007) K^+$
-	1.8e-02 ± 0.4e-02	-	$B^+ \to \bar{D}^*(2007)\pi^+\pi^+\pi^-\pi^0$

Table 3.3: Changes in the branching fractions of the B_s^0 meson

BR before	BR after	Change in %	Decay channel
2.2e-04 ± 0.9e-04	2.2e-04 ± 0.6e-04	± 0	$B_s^0 \to D^+D-$
4.0e-03 ± 0.9e-03	4.4e-03 ± 0.5e-03	+10.0	$B_s^0 \to D_s^+D_s^-$
1.88e-02 ± 0.34e-02	1.86e-02 ± 0.30e-02	-1.1	$B_s^0 \to D_s^{*+}D_s^{*-}$
3.63e-04 ± 1.3e-04	2.8e-04 ± 0.5e-04	-22.9	$B_s^0 \to D_s^+D^-$
1.9e-04 ± 0.39e-04	2.03e-04 ± 0.28e-04	+6.8	$B_s^0 \to D_s^-K^+$
3.42e-04 ± 1.41e-04	3.3e-04 ± 0.4e-04	-3.5	$B_s^0 \to J/\psi(1S)\eta'$
0.95e-06 ± 0.34e-06	7.6e-07 ± 1.9e-07	-20.0	$B_s^0 \to \pi^+\pi^-$
5.10e-04 ± 1.99e-04	3.9e-04 ± 0.7e-04	-23.5	$B_s^0 \to J/\psi(1S)\eta$
1.050e-03 ± 0.105e-03	1.08e-03 ± 0.09e-03	+2.9	$B_s^0 \to J/\psi(1S)\phi(1020)$
1.97e-05 ± 0.44e-05	1.87e-05 ± 0.17e-05	-5.1	$B_s^0 \to J/\psi(1S)K_s^0$
4.4e-05 ± 1.3e-05	4.4e-05 ± 0.9e-05	± 0	$B_s^0 \to J/\psi(1S)K^*(892)$
2.61e-04 ± 0.92e-04	2.6e-04 ± 0.6e-04	-0.4	$B_s^0 \to J/\psi(1S)f_2(1525)$
1.39e-04 ± 0.14e-04	1.35e-04 ± 0.16e-04	-2.9	$B_s^0 \to f_0(980)J/\psi(1S)$
7.70e-04 ± 1.07e-04	7.9e-04 ± 0.7e-04	+2.6	$B_s^0 \to J/\psi(1S)K^+K^-$
3.1e-04 ± 1.7e-04	3.3e-04 ± 0.9e-04	+6.5	$B_s^0 \to \psi(2S)\eta$
7.1e-05 ± 1.8e-05	7.3e-05 ± 1.3e-05	+2.8	$B_s^0 \to \psi(2S)\pi^+\pi^-$
5.13e-04 ± 0.8e-04	5.4e-04 ± 0.6e-04	+1.9	$B_s^0 \to \psi(2S)\phi$
2.1e-03 ± 0.6e-03	2.05e-03 ± 0.31e-03	-2.4	$B_s^0 \to D_s^{*-}\pi^+$
2.95e-03 ± 0.44e-03	3.04e-03 ± 0.23e-03	+3.0	$B_s^0 \to D_s^-\pi^+$
7.4e-03 ± 1.7e-03	7.0e-03 ± 1.5e-03	-5.4	$B_s^0 \to D_s^-\rho^+(770)$
1.03e-02 ± 0.26e-02	9.7e-03 ± 2.2e-03	-5.8	$B_s^0 \to D_s^{*-}\rho^+(770)$
6.5e-03 ± 1.2e-03	6.3e-03 ± 1.1e-03	-3.1	$B_s^0 \to D_s^-\pi^+\pi^+\pi^-$
2.64e-05 ± 0.28e-05	2.5e-05 ± 0.17e-05	-5.3	$B_s^0 \to K^+K^-$
5.3e-06 ± 1.0e-06	5.5e-06 ± 0.6e-06	+3.8	$B_s^0 \to K^-\pi^+$
1.10e-06 ± 0.24e-06	1.13e-06 ± 0.30e-06	+2.7	$B_s^0 \to K^*(892)\phi$
3.5e-05 ± 0.4e-05	3.52e-05 ± 0.34e-05	+0.6	$B_s^0 \to \phi\gamma$
2.81e-05 ± 1.25e-05	2.8e-05 ± 0.7e-05	-0.4	$B_s^0 \to K^*(892)\bar{K}^*(892)$
1.9e-05 ± 0.6e-05	1.93e-05 ± 0.31e-05	+1.6	$B_s^0 \to \phi\phi$

3.2 Implementation of form factor models

In addition to the branching ratios, it is possible to update current form factor parametrizations and to implement new ones within the HADRONS++ module. The new/updated form factor models are mainly picked from BaBar[20] and Belle[21]. Both are experiments which are dedicated to studying B-meson characteristics such as CP violation and rare decays, but also to thoroughly investigating the form factors. Mostly, the differential partial decay widths $\mathrm{d}\Gamma_i$ are calculated in dependency of various variables such as the momentum transfer q. The former experiment is located in the SLAC National Accelerator Laboratory in Menlo Park, USA, whereas the latter is located at the High Energy Accelerator Research Organisation in Tsubaka, Japan. Both have been measuring data since 1999, but BaBar's runtime ended in 2008. The PEP-II B Factory of BaBar is a $\mathrm{e}^+\mathrm{e}^-$ collider operating at a center of mass energy of 10.58 GeV which is the threshold of the $\Upsilon(4S)$ (Upsilon meson) resonance. The reason for this is that the $\Upsilon(4S)$, which consists of $(b\bar{b})$, decays almost solely into $B^0\bar{B}^0$ or B^+B^- and therefore provides a very good source for producing B-mesons. The Belle experiment works in a similar fashion to BaBar, but the accelerator is called KEK-B-factory. Since the focus of this thesis is on individual decays, it is not necessary to examine and simulate the full collider.

3.2.1 The BGL model

The implementation of the BGL model will be done for the $B \to \pi$, $B \to \eta$ and $B \to D$ transitions. The new form factor model will be stored in the `Current_Library`. If the model of the $P \to P'$ current in the decay channel is set to `FORM_FACTOR = 9`, the BGL parametrization will be used.

$B \to \pi$ mode

The BaBar collaboration[22] evaluated and published measurements of $B \to \pi l \nu_l$ and $B^+ \to \eta l^+ \nu_l$ decays in 2012. The partial branching fractions were measured as a function of the squared momentum transfer q^2. Furthermore, the coefficients needed for the BGL model were fitted with the help of the obtained data. Fig. 3.1 shows the partial branching ratios $\Delta\mathcal{B}/\Delta q^2$ as a function of q^2, divided into 12 bins for the $B^0 \to \pi^- l^+ \nu_l$ decay (blue dots) and 11 bins for the $B^+ \to \pi^0 l^+ \nu_l$ decay (red dots). The data presented is unfolded which means that the detector effects have been corrected for showing the actual q^2. The bigger error bars on the y-axis are statistical and systematic uncertainties combined, whereas the smaller one considers only the statistical uncertainties. The uncertainties for the x-axis are determined by the bin widths, hence they are ± 1 GeV^2 except for the last data points with ± 2 GeV^2 or ± 3 GeV^2. In addition, the BGL parametrizations

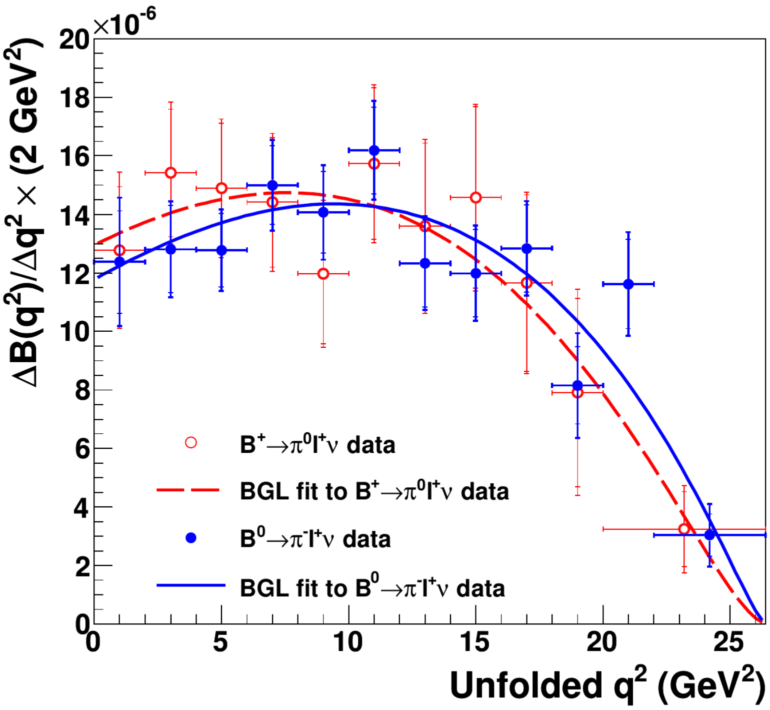

Figure 3.1: The partial branching ratios for the $B^0 \to \pi^- l^+ \nu_l$ (blue dots) and $B^+ \to \pi^0 l^+ \nu_l$ (red dots) decays are displayed in 12 or 11 bins where the bin widths also represent the uncertainties of q^2. The bin widths are 2 GeV^2 except for the last bins with 4 GeV^2 or 6 GeV^2. Furthermore, the BGL fits to both channels are shown.[22]

which are fitted to the experimental data are plotted with $k_{\text{max}} = 2$. The fitted values a_1/a_0 and a_2/a_0 with their respective uncertainties are shown in Tab. 3.4. The coefficient $a_0 = (2.26 \pm 0.20) \cdot 10^{-2}$ applies to both decay channels.

Table 3.4: The fit parameters a_1 and a_2 are shown in dependency of a_0.[22]

Decay channel	a_1/a_0	a_2/a_0
$B^0 \to \pi^- l^+ \nu_l$	-1.15 ± 0.19	-4.52 ± 1.03
$B^+ \to \pi^0 l^+ \nu_l$	-0.63 ± 0.30	-5.80 ± 1.24

The values, as presented in Tab. 3.4, are implemented for f_+ in SHERPA. f_0 is set to zero which is valid for $P \to P' l \nu_l$ decays (see chapter 2.4). The Blaschke factor in this case reads $P(q^2) = z(q^2, m_{B^*})$ to regard the pole at $q^2 = m_{B^*}$. The free parameter t_0 is set to $t_0 = 0.65 \cdot t_-$ as suggested in[23].

$B \to \eta$ mode

The $B \to \eta$ current involves a $b \to u$ transition similar to the $B \to \pi$ current. The η meson itself is a mixture of $u\bar{u}$, $d\bar{d}$ and $s\bar{s}$. In the reference[24], the form factor f_+ is derived from light-cone sum rules (LCSRs). The method uses a series expansion of the correlation function which in this case reads[24]:

$$\Pi_\mu^P(p,q) = i \int e^{i(qx)} \langle P(p)| T[\bar{u}\gamma_\mu b](x) j_B^\dagger(0) |0\rangle \, \mathrm{d}^4x \tag{3.1}$$

with $j_B^\dagger := m_b \bar{u} i\gamma_5 b$ and T being a coefficient function. Since the integral contains information about the hadronic current, the form factor f_+ can be derived from it. The sum rule was performed on f_+ and has its application region in $0 < q^2 < 16$ GeV^2. The other form factor f_0 is defined as zero again. The approach of the authors was to fit the BGL model on top the parametrization gained from LCSRs and afterwards to extrapolate the BGL parametrization until $q^2_{\max} = (m_B - m_\eta)^2$ is reached. Since the series expansion converges very fast[24], it is truncated after $k = 3$. The coefficients needed for the BGL parametrization are displayed together with the fit outcomes from BaBar[22] in Tab. 3.5. For the implementation, $t_0 = 14.14$ GeV^2, as proposed in reference[24], is used. By doing this, z becomes fairly small with $|z| < 0.13$. As for the Blaschke factor, it remains the same as above which means that it takes the single pole at m_{B^*} into account.

Table 3.5: BGL fit parameters for the $B \to \eta$ transition obtained from light-cone sum rules[24] and from fits to measurements[22].

Coefficients	Obtained from LCSRs	Obtained from BaBar 2012
a_0	0.0031 $\pm$ 0.0003	0.0031 $\pm$ 0.0003
a_1	-0.0090 $\mp$ 0.0034	-0.005301 $\mp$ 0.002697
a_2	0.00243 $\pm$ 0.0172	
a_3	-0.0908 $\mp$ 0.0039	

$B \to D$ mode

At the end of 2015, the Belle collaboration[25] published updated measurements regarding $B \to D l \nu_l$ decays and also published fit parameters for the BGL model. In this case, the differential decay width $\mathrm{d}\Gamma/\mathrm{d}w$ were measured. The relation between the kinematic variables w and q^2 can be found in equation (2.10). The fit results of the BGL series (black line) to the experimental data of Belle (blue) combined with lattice QCD calculations (green and purple) are illustrated in Fig. 3.2. The bin widths of 0.3 represent the horizontal error bars. The limits of w are determined by q^2 which means that $w_{\min} = 1$ results from $q^2_{\max} = (m_{B^+} - m_{\bar{D}^0})^2$ and $w_{\max} \approx 1.6$ originates from $q^2_{\min} = 0$. The grey region in Fig. 3.2 displays the uncertainties of the coefficients of the BGL parametrization with $k_{\max} = 3$. However, the computations of the parameters were also done for $k_{\max} = 2$. For the form factors f_+ and f_0, the results of $k_{\max} = 2$ and $k_{\max} = 3$ are shown in Tab. 3.6 with their respective uncertainties. Regarding the implementation, $k_{\max} = 3$ is chosen to achieve the highest accuracy. The Blaschke factors are $P_0 = P_+ = 1$ as suggested in [25] and the arbitrary functions ϕ_+ and ϕ_0 have the form[26]:

$$\phi_+(z) = 1.1213(1+z)^2(1-z)^{1/2}\left[(1+r)(1-z)+2\sqrt{r}(1+z)\right]^{-5} \tag{3.2}$$

$$\phi_0(z) = 0.5299(1+z)(1-z)^{3/2}\left[(1+r)(1-z)+2\sqrt{r}(1+z)\right]^{-4} \tag{3.3}$$

where $r := m_B/m_D$.

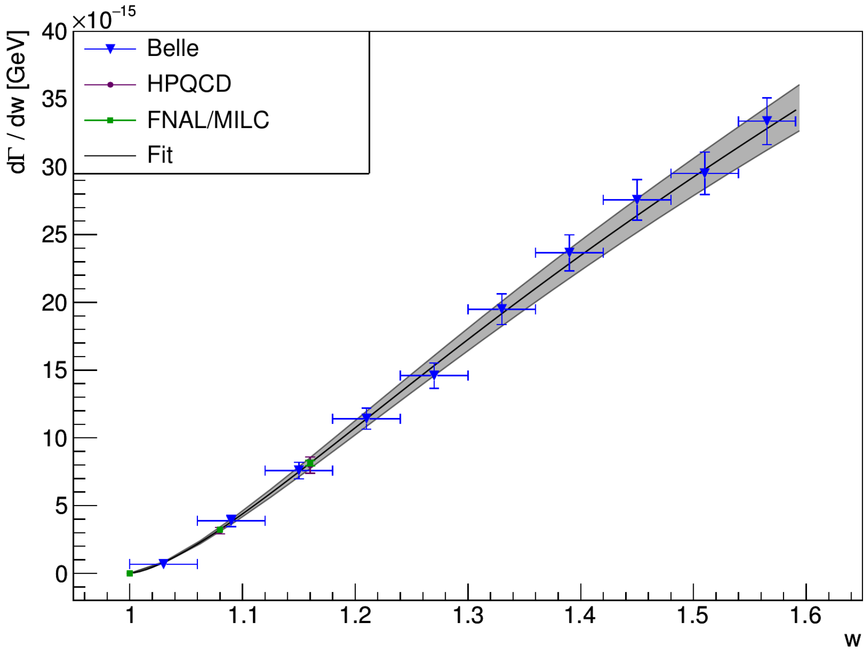

Figure 3.2: $B \to Dl\nu_l$; The measured data for the differential decay width (blue points) are shown in dependency of w together with the lattice QCD (FNAL/MILC and HPQCD). Both have been used for the BGL fit which is portrayed by the black line. The graph in this diagram only represents f_+. The grey areas point out the uncertainties of the parameters used for the BGL model.[25]

Table 3.6: Fit parameters for the BGL model with the series being truncated after $k = 2$ and $k = 3$.[25]

Coefficients	$k_{\text{max}} = 2$	$k_{\text{max}} = 3$
$a_{+,0}$	0.0127 ± 0.0001	0.0126 ± 0.0001
$a_{+,1}$	-0.091 ± 0.002	-0.094 ± 0.003
$a_{+,2}$	0.34 ± 0.03	0.034 ± 0.04
$a_{+,3}$		-0.1 ± 0.6
$a_{0,0}$	0.0115 ± 0.0001	0.0115 ± 0.0001
$a_{0,1}$	-0.058 ± 0.002	-0.057 ± 0.002
$a_{0,2}$	0.22 ± 0.02	0.12 ± 0.04
$a_{0,3}$		0.4 ± 0.7

3.2.2 Refreshing the CLN model

Over time, more precise measurements of $B \to D^{(*)} l\nu$ decays have been published. Since the CLN model (referred to as HQET2 in SHERPA) has a few fit parameters which depend on experimental results, the parameters were recalculated specifically for the $B \to D$ and $B \to D^*$ transitions. For the former, the free parameters ρ^2 and $V_1(1)$ of equation (2.22) are changed to:

- ρ^2: $1.19 \to 1.09 \pm 0.05$
- $V_1(1)$: $0.98 \to 1.0541 \pm 0.0083$

in SHERPA. ρ^2 is taken from Belle[25] and $V_1(1)$ is taken from the Fermilab Lattice and MILC Collaborations[26]. For the latter, the fit values ρ^2, $R_1(1)$, $R_2(2)$ and the normalization parameter h_{A1}, which are used in the equations (2.27-2.29), are adjusted to[27]:

- ρ^2: $1.34 \to 1.214 \pm 0.034 \pm 0.009$
- $R_1(1)$: $1.18 \to 1.401 \pm 0.034 \pm 0.018$
- $R_2(1)$: $0.71 \to 0.864 \pm 0.024 \pm 0.008$
- h_{A1}: $0.91 \to 0.921 \pm 0.013 \pm 0.020$

The former uncertainty is systematical whereas the latter is of statistical nature.

4 Results and discussion

The HADRONS++ module simulates the hadron decay according to the given branching ratios and continues the decay process until stable particles are reached (full decay). Alternatively, it simulates the decay by using only one specific decay channel (single decay). In this chapter, all simulations are done with the SHERPA SVN revision 28335.

4.1 Testing the full decay kinematics

The full decay simulation is used to check how significant the improvements are with the updated branching fractions, since the full decay depends on them. Because the `Decays.dat` files for B mesons are far from being completed, the leftover branching ratios have to be filled with the help of partonic decays. Therefore, the parton shower and hadronisation modules simulate the remaining unknown variables by creating parton showers followed by hadronisation processes.

Due to the fact that most of the direct decay products of the B meson are highly unstable, a decay cascade evolves, and it is necessary to set a limit, whether the products will decay further or not. Marked as stable in the simulation are those with a mean free path of more than 10 mm because those will then interact with the detector material. The count of stable particles which resulted from the whole decay process including the decay cascade is referred to as multiplicity and it can be calculated in the full decay simulation. Labelled as stable in the decay cascade are e.g. $\pi^{\pm}$, $e^{\pm}$ and $\mu^{\pm}$. Examples for unstable particles are π^0 and D mesons. To ensure reasonable statistics, one million decays of B^+ have been simulated. Then, the statistical uncertainties are negligible which can be seen in the appendix A.1.

The counts of the e^+ and π^+ are pictured in Fig. 4.1 as histograms, where the black line represents the old data and red the new one. In most decays, no positrons will be created and in approximately 300,000 events only one positron per event will be generated. Obviously, the outcomes do not differ a lot from each other, since the implemented changes are small. Nonetheless, the produced positrons are slightly fewer than before, most likely due to the decreased branching fraction of the $B^+ \to D^* l^+ \nu_l$ channel. The same can be said for the μ^+ because they share the same branching ratios. Now looking at the π^+, its multiplicity is significantly higher than the multiplicity of the positron. Most of

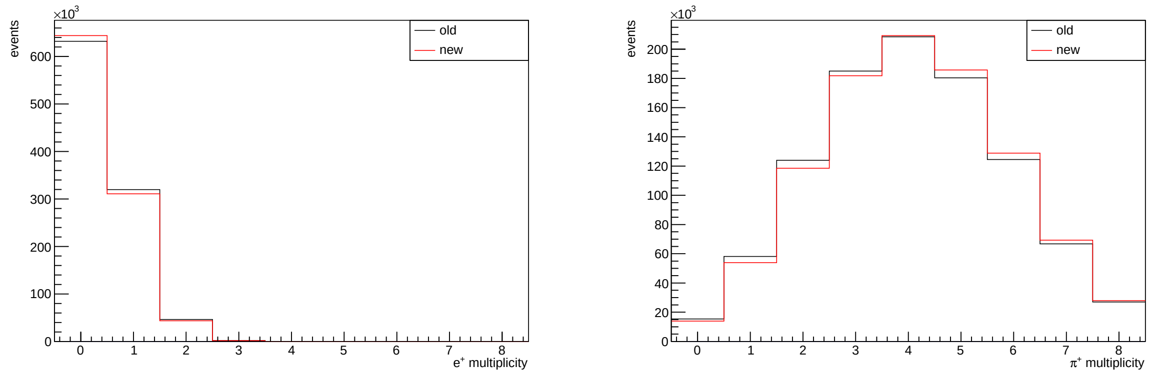

Figure 4.1: Comparison of the old and new multiplicities of e^+ (left) and π^+ (right) with a simulation of one million B^+ decays.

the mesons which are direct products of the B^+ meson are highly unstable and decay further until they reach a stable point. In most cases, it is the π^+ which is why the multiplicity of it is high with a peak of four π^+ being produced in one event. With the updated data, the overall multiplicity is slightly increased due to the newly implemented $B^+ \to \bar{D}^*(2007)\pi^+\pi^+\pi^-\pi^0$ decay channel.
Beyond that, the full decay simulation computes the normalized differential decay widths $\frac{1}{\Gamma}\frac{\mathrm{d}\Gamma}{\mathrm{d}E}$ in dependency of the energies E of the particles. For a three-body decay and higher body decay, the kinematics of the resulting products have to be generated non-isotropically because of the numerous degrees of freedom as discussed in chapter 2.2. Therefore, the distributions can not take on the form of a delta-distribution, instead the shape is broad. The energies can be viewed in two different ways. One way is to only regard the decay products that are created as a direct result from the initial decaying particle (direct energy) which is shown for the products e^+ and π^+ in Fig. 4.2.

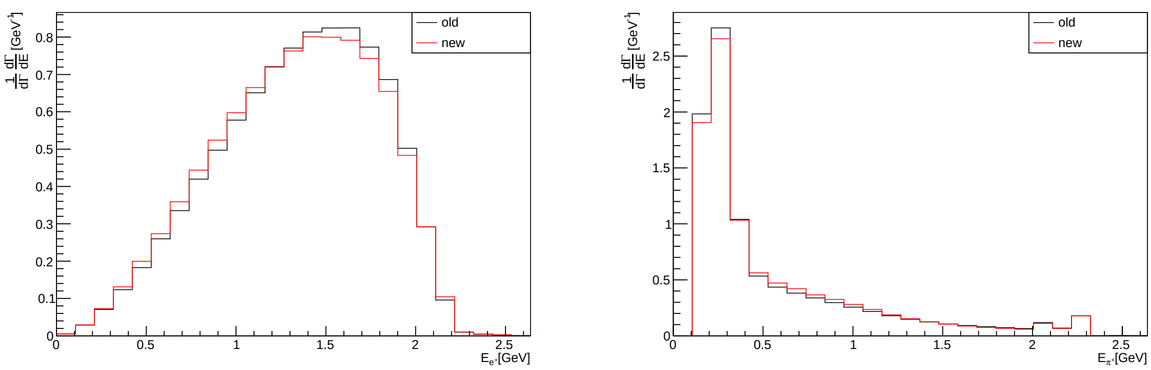

Figure 4.2: Comparison of the old and new differential decay width $\frac{1}{\Gamma}\frac{\mathrm{d}\Gamma}{\mathrm{d}E}$ of e^+ (left) and π^+ (right) with a simulation of one million B^+ decays.

The left histogram shows entries from 0 to 2.5 GeV with a peak around 1.5 GeV. The highest energies of e^+ can be found in $B^+ \to \pi^0 e^+ \nu_e$ decays because the pion is the lightest meson with a mass of around 0.14 GeV. If the π^0 is produced at rest, the positron and the electron-neutrino have about 5.15 GeV to share. Due to the momentum conservation,

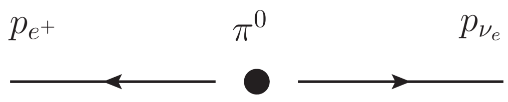

Figure 4.3: Rest frame of the π^0

the momenta of e^+ and ν_e, which are illustrated in Fig. 4.3, have to point in opposite directions and have to have the same lengths. If the masses are neglected, both have roughly the energy of:

$$E = \sqrt{\vec{p}^2 + m^2} \approx |\vec{p}| \approx 2.58 \text{ GeV} \tag{4.1}$$

which is what sets the upper limit in Fig. 4.2 for the positron. As expected, the simulated values for $\mathrm{d}\Gamma/\mathrm{d}E$ are reduced with the new data because of the overall reduced numbers of positrons being generated in the events. Analysing the right histogram in Fig. 4.2, almost all of the produced π^+ have very low energies near the rest energy of 0.14 GeV. The reason is that in most cases they come in groups of three or more beside a D meson which already weighs about 2 GeV.
The other way is to include the particles which are caused by secondary decays into the calculation which are shown in Fig. 4.4 for e^+ and π^+ respectively. With secondary processes, the overall amount of positrons and pions is increased. The more branches the initial decaying particle has, the less energy remains for each final product at the end. This is the reason why the spectrum in respect of the e^+ is much wider with a lot of positrons emerging at low energies, if secondary events are included. The shape of $\mathrm{d}\Gamma/\mathrm{d}E$ in regards to the π^+ stays nearly the same, but with more entries in the lower area.

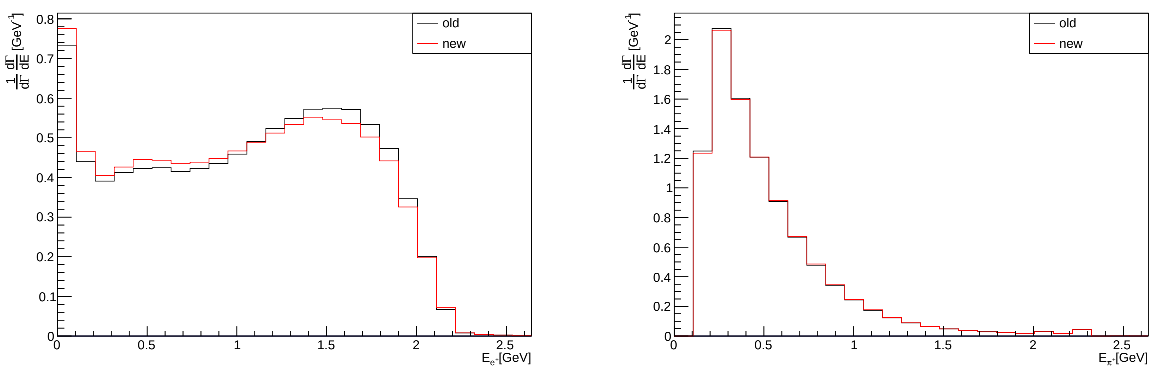

Figure 4.4: Comparison of the old and new differential decay width $\frac{1}{\Gamma}\frac{\mathrm{d}\Gamma}{\mathrm{d}E}$ of e^+ (left) and π^+ (right) with a simulation of one million B^+ decays, but now including those that are produced from secondary decays.

4.2 Analysis of single decay kinematics

To analyse how well the new BGL and the updated HQET2 models behave, they will be used in the single decay simulation against various other form factor models, which were already implemented in SHERPA, as well as experimental data. The latter will be the reference. Therefore, the BGL model will be tested in the $B^0 \to \pi^- e^+ \nu_e$, $B^+ \to \pi^0 e^+ \nu_e$ and $B^+ \to \eta e^+ \nu_e$ decay channels. As for the HQET2 update, it will be analyzed in the $B^+ \to \bar{D}^0 e^+ \nu_e$ and $B^0 \to D^{*-} e^+ \nu_e$ channel. To get a useful comparison between the data and the plotted histograms, all of them will be normalized to have a summed area of one. Afterwards the chi-squared test will be applied. The basic concept of the method is to weight the sum of the squared differences between the expected values x_i and observed results y_i. The weighting is usually done with the variance σ^2:

$$\chi^2 = \sum_{i=1}^{n} \frac{(x_i - y_i)^2}{\sigma^2} = \sum_{i=1}^{n} \frac{(x_i - y_i)^2}{(\Delta y_i)^2} \tag{4.2}$$

Instead of σ^2, only the squared vertical errors $(\Delta y_i)^2$ of the measurements will be used because the uncertainties of the simulations can be neglected for high event numbers. With that in mind, all histograms will be created with one million B decays.

4.2.1 $B^0 \to \pi^- e^+ \nu_e$ / $B^+ \to \pi^0 e^+ \nu_e$ kinematics

The $\mathrm{d}\Gamma/\mathrm{d}q^2$ distributions for the $B^0 \to \pi^- e^+ \nu_e$ (a) and $B^+ \to \pi^0 e^+ \nu_e$ (b) channels are displayed in Fig. 4.5. The BGL implementation (red) is compared against the ISGW[11] (green), ISGW2[28] (violet) and pole fit (blue) model. More information about the latter can be found in the appendix A.2. The blue dots with their respective uncertainties are gathered from BaBar[22]. The vertical error bars are systematical and statistical errors together, whereas the horizontal error bars are the bin widths. The simulations are aligned to have the same binning as the data which means 12 bins for (a) and 11 bins for (b). The obtained χ^2 tests are listed in Tab. 4.1.

Table 4.1: Chi-squared test outcomes for ISGW, ISGW2, pole fit and BGL.

form factor model	**χ^2 test for (a)**	**χ^2 test for (b)**
ISGW	59.12	31.21
ISGW2	31.58	4.33
pole fit	13.38	10.75
BGL	10.19	5.70

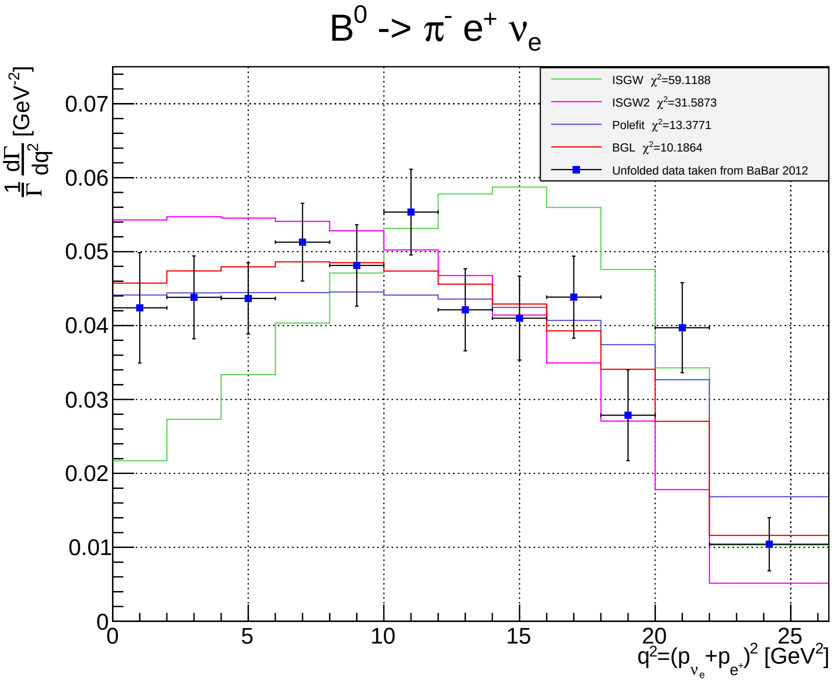

(a)

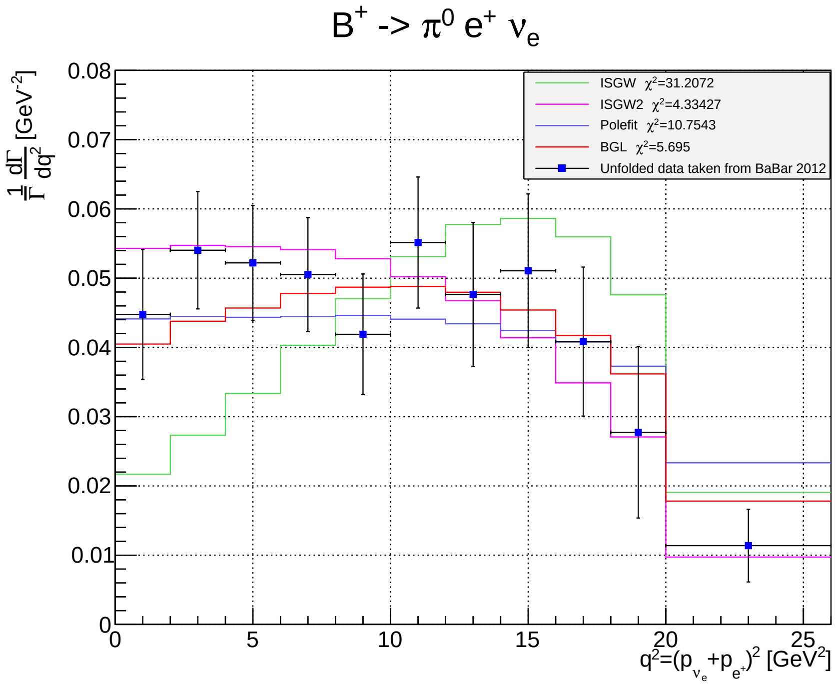

(b)

Figure 4.5: With SHERPA, the normalized $\mathrm{d}\Gamma/\mathrm{d}q^2$ distributions are plotted for the $B^0 \to \pi^- e^+ \nu_e$ (a) and $B^+ \to \pi^0 e^+ \nu_e$ (b) decay channels. The form factor models chosen are: ISGW (green), ISGW2 (violet), pole fit (blue) and BGL (red). The experimental data [22] (blue dots) with their related uncertainties are also shown to provide a reference. The plots, created from SHERPA, have either 12 (a) or 11 (b) bins to match the data.

Starting with (a), it is noticeable that ISGW (green) does not represent the data very well, hence the χ^2 method outputs a high value of 59.12. The ISGW2 (violet), which is the standard setting, matches the actual distribution better ($\chi^2 = 31.58$), but is still not sufficient. With $\chi^2 = 13.38$, the pole fit model suits the data quite well, despite being not set as the default for this channel. Analyzing the BGL parametrization, the chi-squared test yields $\chi^2 = 10.19$. Therefore, the BGL model is chosen as the standard form factor model for this and for the $B^0 \to \pi^-\mu^+\nu_\mu$ channel, since both decay channels show very similar behaviour. Now evaluating (b), it is important to mention that the uncertainties of the data are significantly higher, therefore the chi-squared test generally outputs smaller values. Once more, the ISGW parametrization shows odd behavior and does not fit the experimental observation. With $\chi^2 = 31.21$, the result is not adequate. The pole fit is decent with $\chi^2 = 10.75$, but only due to the uncertainties being so high. In contrast, the ISGW2 matches the data very well with $\chi^2 = 4.33$, which is even better than the $\chi^2 = 5.70$ resulting from BGL. As a consequence, the ISGW2 model remains the default.

4.2.2 $B^+ \to \eta e^+\nu_e$ kinematics

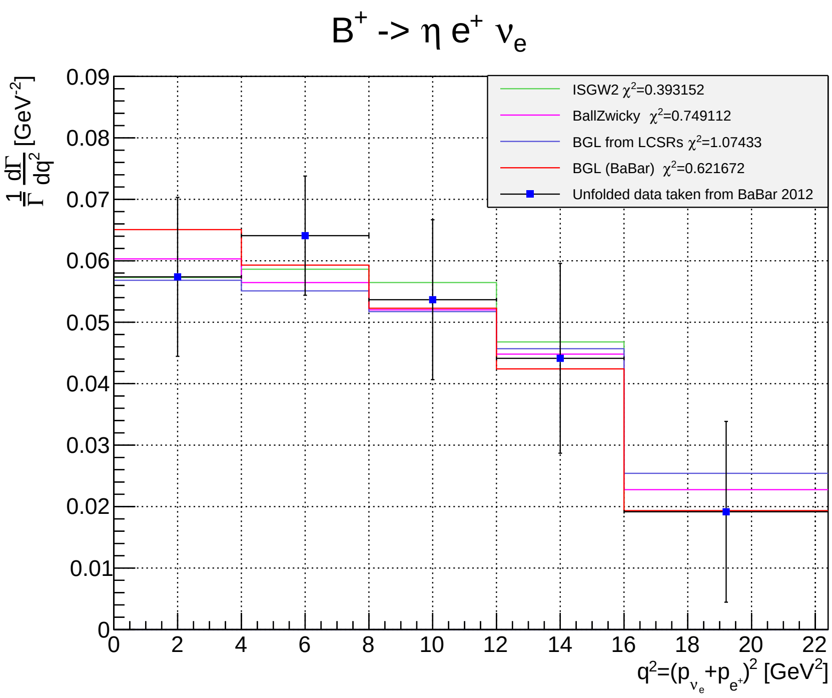

Figure 4.6: The normalized $\mathrm{d}\Gamma/\mathrm{d}q^2$ distributions are plotted for the $B^+ \to \eta e^+\nu_e$ decay channel. The form factor models chosen are: ISGW2 (green), BallZwicky (violet), BGL derived LCSRs (blue) and BGL (BaBar) (red). The data (blue dots) are also taken from [22]. All plots are matched to have the same binning as the data. The bin widths also represent the horizontal uncertainties, whereas the vertical uncertainties are systematical and statistical combined.

In this test, the models ISGW2[28] , Ball and Zwicky[29], BGL gathered from LCSRs and BGL from BaBar are picked and are drawn in Fig. 4.6, together with the data extracted from [22]. The respective χ^2 tests are listed in Tab. 4.2.

Table 4.2: Chi-squared test for ISGW2, Ball and Zwicky, BGL gathered from LCSRs and BGL fit from BaBar

form factor model	$\boldsymbol{\chi^2}$ **test**
ISGW2	0.39
BallZwicky	0.75
BGL from LCSRs	1.07
BGL (BaBar)	0.62

The Ball and Zwicky parametrization (violet) is derived from light-cone sum rules, just like the former BGL model (blue). As it stands, the measurements of $\mathrm{d}\Gamma/\mathrm{d}q^2$ are not good enough to draw reasonable conclusions from the χ^2 test, since there are only five data points with fairly high uncertainties. Nonetheless, the distribution with ISGW2 (green), which is already the default, has the lowest value with $\chi^2 = 0.39$ which is even lower than the $\chi^2 = 0.62$ obtained from the BGL model (BaBar). Regarding this decay channel, the comparison should be repeated if measurements with better accuracy will be published.

4.2.3 $B^+ \to \bar{D}^0 e^+ \nu_e$ kinematics

The next channel, that is analyzed, is the $B^+ \to \bar{D}^0 e^+ \nu_e$ decay. Taking the data from Belle[25], published in 2015, the comparison is made between the HQET2 (green), the updated HQET2 (violet), the ISGW2 (blue) and the BGL (red) parametrization which are all shown in Fig. 4.7. The calculations gathered from the χ^2 tests are listed in Tab. 4.3. The ISGW2 and the old HQET2 model have a similar goodness of fit with $\chi^2 = 14.08$ for the former and $\chi^2 = 14.55$ for the latter. Comparing the updated HQET2 model against the old version, the chi-squared result is a lot better with $\chi^2 = 8.56$. Thus, the current parameters $\rho^2 = 1.09$ and $V_1(1) = 1.0541$ are kept. Considering the BGL parametrization, the test yields $\chi^2 = 8.98$ which is also a very good value, but the refreshed HQET2 is still better. In conclusion, the HQET2 setting remains with updated parameters.

Table 4.3: Obtained results of the χ^2 tests of HQET2, updated HQET2, ISGW2 and BGL

form factor model	$\boldsymbol{\chi^2}$ **test**
HQET2	14.55
HQET2 (updated)	8.56
ISGW2	14.08
BGL	8.98

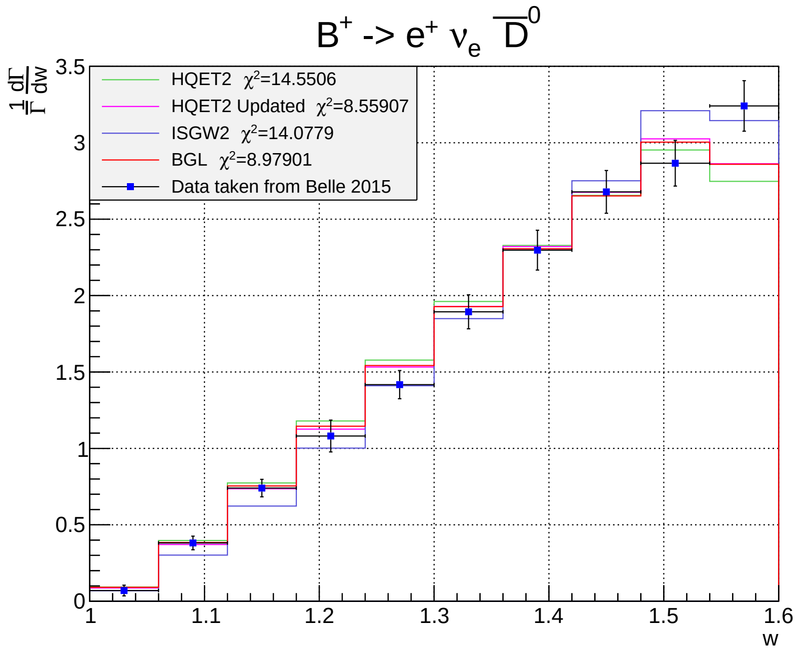

Figure 4.7: The normalized $\mathrm{d}\Gamma/\mathrm{d}w$ distributions are plotted for the $B^+ \to \bar{D}^0 e^+ \nu_e$ decay channel with the HQET2 (green), updated HQET2 (violet), ISGW2 (blue) and BGL model (red). The data (blue dots) are taken from [25]. The bin width is 0.6 and is used as the horizontal uncertainty.

4.2.4 $B^0 \to D^{*-} e^+ \nu_e$ kinematics

The simulation of the $B^0 \to D^{*-} e^+ \nu_e$ decay channel is of particular interest because its branching ratio is very high with $\mathcal{B} = (4.93 \pm 0.11)\%$ [4]. In this analysis, the chosen models are: HQET, HQET2, updated HQET2 and ISGW2. The normalized histograms and the normalized data, are shown in Fig. 4.8. The measurements, taken from Belle[27], are already background subtracted. The vertical uncertainties are not visible in the original paper, hence the size of the dots were taken to represent them. The bin widths are used as horizontal error bars. Because the measurements are only background subtracted and not unfolded, the simulations do not represent the data very well. Perhaps there are some other information missing which would explain the differences between the SHERPA simulation and the experiment.
As it stands, the high deviations translate into bad χ^2 tests. The results are shown in Tab. 4.4. The HQET model with $\chi^2 = 1702$ has the worst accuracy. The distribution is entirely different compared to the measurements. The HQET2 and the updated HQET2 parametrizations do not differ a lot from each other, hence the test for both yields $\chi^2 \approx 830$. With $\chi^2 = 480$, the ISGW2 model matches the data best. As a consequence, the default setting is changed from HQET to ISGW2.

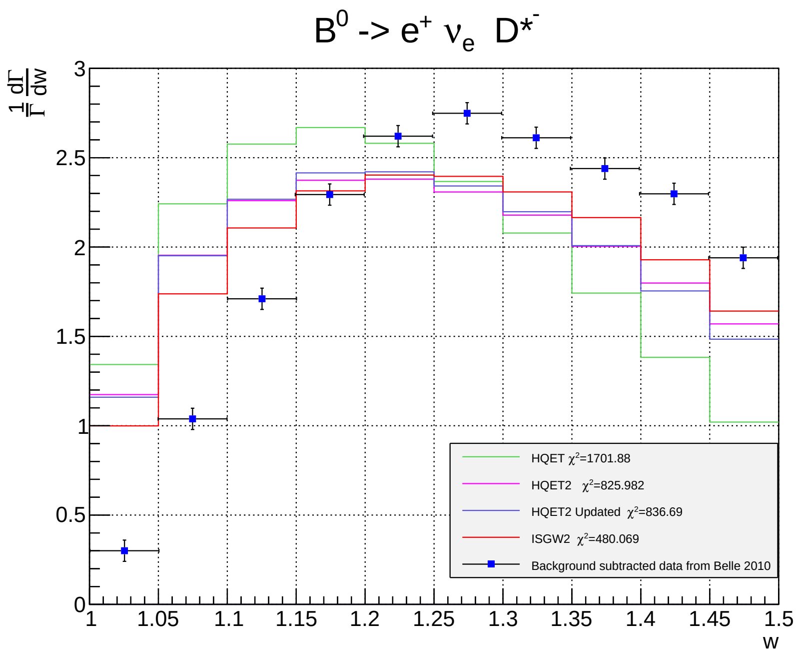

Figure 4.8: $B^0 \to D^{*-}e^+\nu_e$ decay channel; The normalized differential decay widths $\mathrm{d}\Gamma/\mathrm{d}w$ are drawn as histograms with the following form factor parametrizations: HQET, HQET2, updated HQET2 and ISGW2. In addition, the normalized measurements from Belle[27] are shown as reference. The vertical error bars are the dot sizes which were used in the original paper. The horizontal error bars are the bin widths.

Table 4.4: Obtained results of the χ^2 tests of HQET, HQET2, updated HQET2 and ISGW2

form factor model	χ^2 **test**
HQET	1702
HQET2	826
updated HQET2	837
ISGW2	480

5 Summary and outlook

The simulation of B meson decays could be improved in several areas. Updating the branching fractions resulted in small changes in the full decay simulation. For example, the multiplicity of the e^+ has been decreased, whereas the multiplicity of the π^+ has been increased. Slight differences in the differential decay widths $\mathrm{d}\Gamma/\mathrm{d}E$ in respect of the end products were noticeable too. The performed adjustments led to more accurate decay simulations of B meson decays because the current branching ratios used have significantly lower uncertainties.
Regarding the implementation of the BGL model, the calculated decay kinematics represented the data in most cases well. As a consequence, the form factor model is now the default setting for $B^0 \to \pi^- e^+ \nu_e$ and $B^0 \to \pi^- \mu^+ \nu_\mu$ decays. Regarding the $B^+ \to \pi^0 e^+ \nu_e$ decay, the ISGW2 model is unchanged since it matches the current measurements from BaBar well. The comparison in the $B^+ \to \eta e^+ \nu_e$ channel showed that the chosen models ISGW2, Ball and Zwicky and BGL all come very close to the data. In the end, the ISGW2 model remains the default. Due to the reason that the data which were used have high uncertainties, the test should be repeated with more accurate measurements. Refreshing the parameters of the HQET2 model for $P \to P'$ transitions resulted in a significant improvement in the $B^+ \to \bar{D}^0 e^+ \nu_e$ decay channel and therefore the updated parameters were kept. The new HQET2 fit parameters for $P \to V$ transitions could not be thoroughly analyzed because the SHERPA software could not reproduce the data regardless of the chosen form factor models. Nonetheless, the outcome was that the ISGW2 model fits the present measurements best, hence it is now the default.
Collision simulations in which B mesons appear as intermediate products can benefit from the improved B meson decay simulation. For the future, more branching fractions should be updated to further improve the simulation. If better measurements of B meson decays will be published, it is possible that there will be updated fit parameters available for certain form factor models too. Then, the parameters could be implemented in SHERPA and new comparisons between several form factor parametrizations could be done again.

A Appendix

A.1 Statistical uncertainties in the full decay simulation

In Fig. A.1, the statistical uncertainties are shown in the histograms for the B^+ events in dependency of the e^+ multiplicity (left) and for the normalized differential decay width $\frac{1}{\Gamma}\frac{\mathrm{d}\Gamma}{\mathrm{d}E}$ in respect of the direct energy (right). The histograms were created with one million B^+ decay events. The vertical error bars are smaller than the visible differences between the old and new data. The horizontal error bars are the bin widths.

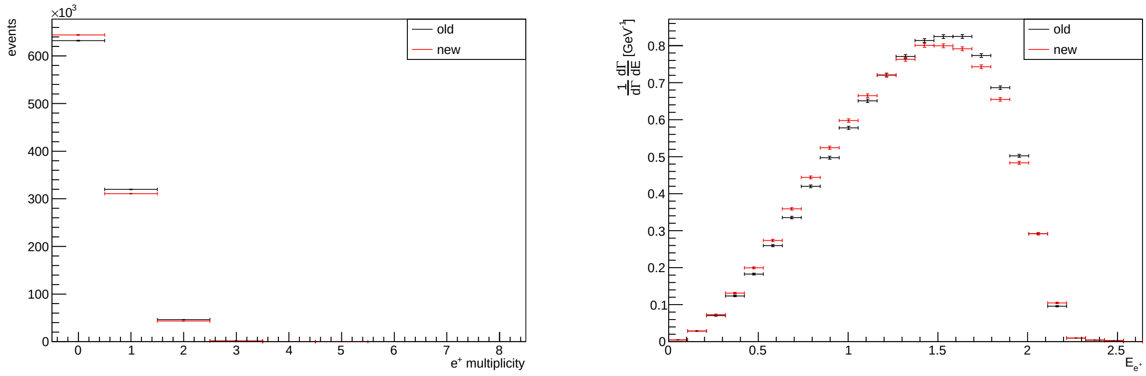

Figure A.1: Excerpt of the B^+ full decay simulation with one million events; The statistical uncertainties are displayed for the event numbers in dependency of the e^+ multiplicity and for the differential decay width $\frac{1}{\Gamma}\frac{\mathrm{d}\Gamma}{\mathrm{d}E}$ (direct energy). The bin widths represent the horizontal error bars.

A.2 The pole fit model

An approach to parametrize the form factors f_i is a pole fit which can take various resonances in the decay channel into account[5]:

$$\begin{aligned} f_i(q^2) =& \frac{F_0}{1 + a_0\frac{q^2}{m_0^2} + b_0\left(\frac{q^2}{m_0^2}\right)^2 + c_0\left(\frac{q^2}{m_0^2}\right)^3 + d_0\left(\frac{q^2}{m_0^2}\right)^4} \\ &+ \frac{F_1}{1 + a_1\frac{q^2}{m_1^2} + b_1\left(\frac{q^2}{m_1^2}\right)^2 + c_1\left(\frac{q^2}{m_1^2}\right)^3 + d_1\left(\frac{q^2}{m_1^2}\right)^4} \end{aligned} \tag{A.1}$$

For the $B \to \pi$ transition the equation for f_+ reduces to[30]:

$$f_+(q^2) = \frac{F_0}{1 + a_0 \frac{q^2}{m_0^2}} + \frac{F_1}{1 + a_1 \frac{q^2}{m_1^2}} \tag{A.2}$$

The parameters are as follows:

$$a_0 = a_1 = -1 \tag{A.3}$$
$$F_0 = 0.744 \tag{A.4}$$
$$m_0 = 5.32 \text{ GeV} \tag{A.5}$$
$$F_1 = -0.486 \tag{A.6}$$
$$m_1 = 6.382 \text{ GeV} \tag{A.7}$$

F_0, F_1 and m_1 are fit parameters and m_0 represents the $q^2 = m_{B^*}$ resonance. In the case of f_0, the equation reads[30]:

$$f_0(q^2) = \frac{F_0}{1 + a_0 \frac{q^2}{m_0^2}} \tag{A.8}$$

with the fit parameters given as:

$$a_0 = -1 \tag{A.9}$$
$$F_0 = 0.258 \tag{A.10}$$
$$m_0 = 5.815 \text{ GeV} \tag{A.11}$$

References

[1] T. Sjöstrand, S. Mrenna and P. Skands, *A brief introduction to PYTHIA 8.1*, Computer Physics Communications **178** (2008), no. 11, 852 – 867.

[2] T. Gleisberg, S. Höche, F. Krauss, M. Schönherr, S. Schumann, F. Siegert and J. Winter, *Event generation with SHERPA 1.1*, Journal of High Energy Physics **2009** (2009), no. 02, 007.

[3] E. ATLAS, *An ATLAS event with 4 muons*, General Photo, Apr 2014.

[4] K. O. et al. (Particle Data Group), *Review of Particle Physics*, Chinese Physics C **38** (2016), .

[5] F. Siegert, *Simulation of hadron decays in SHERPA*, Diplomarbeit, TU Dresden, Germany, 2007.

[6] M. Thomson, *Modern particle physics*, Cambridge University Press, New York, 2013.

[7] A. Ceccucc, Z. Ligeti and Y. Sakai, *THE CKM QUARK-MIXING MATRIX*, Chinese Physics C **38** (2014), .

[8] M. Mazur, *Study of Exclusive Semileptonic B Meson Decays to Tau Leptons*, Ph.D. thesis, University of California, September 2007.

[9] T. Laubrich, *Implementation of tau-lepton Decays into the Event-Generator SHERPA*, Diplomarbeit, Technische UniversitÃďt Dresden, Germany, March 2006.

[10] M. Wirbel, B. Stech and M. Bauer, *Exclusive semileptonic decays of heavy mesons*, Zeitschrift für Physik C Particles and Fields **29** (1985), no. 4, 637–642.

[11] N. Isgur, D. Scora, B. Grinstein and M. B. Wise, *Semileptonic B and D decays in the quark model*, Phys. Rev. D **39** (1989), 799–818.

[12] I. Caprini, L. Lellouch and M. Neubert, *Dispersive bounds on the shape of anti-B —> D(*) lepton anti-neutrino form-factors*, Nucl. Phys. **B530** (1998), 153–181, [arXiv:hep-ph/9712417 [hep-ph]].

[13] C. G. Boyd, B. Grinstein and R. F. Lebed, *Model independent determinations of anti-B —> D (lepton), D* (lepton) anti-neutrino form-factors*, Nucl. Phys. **B461** (1996), 493–511, [arXiv:hep-ph/9508211 [hep-ph]].

[14] T. Becher and R. J. Hill, *Comment on form-factor shape and extraction of |V(ub)| from B —> pi l nu*, Phys. Lett. **B633** (2006), 61–69, [arXiv:hep-ph/0509090 [hep-ph]].

[15] P. del Amo Sanchez et al., BaBar collaboration, *Study of $B \to \pi\ell\nu$ and $B \to \rho\ell\nu$ Decays and Determination of $|V_{ub}|$*, Phys. Rev. **D83** (2011), 032007, [arXiv:1005.3288 [hep-ex]].

[16] F. Krauss, R. Kuhn and G. Soff, *AMEGIC++ 1.0: A Matrix element generator in C++*, JHEP **02** (2002), 044, [arXiv:hep-ph/0109036 [hep-ph]].

[17] J.-C. Winter, F. Krauss and G. Soff, *A Modified cluster hadronization model*, Eur. Phys. J. **C36** (2004), 381–395, [arXiv:hep-ph/0311085 [hep-ph]].

[18] R. Kleiss, W. J. Stirling and S. D. Ellis, *A New Monte Carlo Treatment of Multiparticle Phase Space at High-energies*, Comput. Phys. Commun. **40** (1986), 359.

[19] D. J. Lange, *The EvtGen particle decay simulation package*, Nucl. Instrum. Meth. **A462** (2001), 152–155.

[20] B. A. et al., *The BABAR detector*, Nuclear Instruments and Methods in Physics Research Section A: Accelerators, Spectrometers, Detectors and Associated Equipment **479** (2002), no. 1, 1 – 116, Detectors for Asymmetric B-factories.

[21] A. A. et al., *The Belle detector*, Nuclear Instruments and Methods in Physics Research Section A: Accelerators, Spectrometers, Detectors and Associated Equipment **479** (2002), no. 1, 117 – 232, Detectors for Asymmetric B-factories.

[22] J. P. Lees et al., BaBar collaboration, *Branching fraction and form-factor shape measurements of exclusive charmless semileptonic B decays, and determination of $|V_{ub}|$*, Phys. Rev. **D86** (2012), 092004, [arXiv:1208.1253 [hep-ex]].

[23] J. A. Bailey et al., *The $B \to \pi\ell\nu$ semileptonic form factor from three-flavor lattice QCD: A Model-independent determination of $|V_{ub}|$*, Phys. Rev. **D79** (2009), 054507, [arXiv:0811.3640 [hep-lat]].

[24] P. Ball and G. W. Jones, *B —> eta-(prime) Form Factors in QCD*, JHEP **08** (2007), 025, [arXiv:0706.3628 [hep-ph]].

[25] R. Glattauer et al., Belle collaboration, *Measurement of the decay $B \to D\ell\nu_\ell$ in fully reconstructed events and determination of the Cabibbo-Kobayashi-Maskawa matrix element $|V_{cb}|$*, Phys. Rev. **D93** (2016), no. 3, 032006, [arXiv:1510.03657 [hep-ex]].

[26] J. A. Bailey et al., MILC collaboration, *$B \to D\ell\nu_\ell$ form factors at nonzero recoil and $|V_{cb}|$ from 2+1-flavor lattice QCD*, Phys. Rev. **D92** (2015), no. 3, 034506, [arXiv:1503.07237 [hep-lat]].

[27] W. Dungel et al., Belle collaboration, *Measurement of the form factors of the decay B0 -> D*- ell+ nu and determination of the CKM matrix element |Vcb|*, Phys. Rev. **D82** (2010), 112007, [arXiv:1010.5620 [hep-ex]].

[28] D. Scora and N. Isgur, *Semileptonic meson decays in the quark model: An update*, Phys. Rev. **D52** (1995), 2783–2812, [arXiv:hep-ph/9503486 [hep-ph]].

[29] P. Ball and R. Zwicky, *B —> pi, K, eta decay formfactors from light-cone sum rules*, Continuous advances in QCD. Proceedings, Conference, Minneapolis, USA, May 13-16, 2004, 2004, pp. 160–169.

[30] P. Ball and R. Zwicky, *New results on $B \to \pi, K, \eta$ decay formfactors from light-cone sum rules*, Phys. Rev. **D71** (2005), 014015, [arXiv:hep-ph/0406232 [hep-ph]].

Erklärung

Hiermit erkläre ich, dass ich diese Arbeit im Rahmen der Betreuung am Institut für Kern- und Teilchenphysik ohne unzulässige Hilfe Dritter verfasst und alle Quellen als solche gekennzeichnet habe.

Kien Dang Tran
Dresden, Mai 2016